Available online at www.sciencedirect.com

ScienceDirect

Procedia Manufacturing 47 (2020) 1178–1183

Procedia MANUFACTURING

www.elsevier.com/locate/procedia

23rd International Conference on Material Forming (ESAFORM 2020)

Prediction of Microstructure Evolution for Additive Manufacturing of Ti-6Al-4V

Xinyu Yang[a,b,c*], Richard A. Barrett[a,b,c], Mingming Tong[a,b,c], Noel M. Harrison[a,b,c], Sean B. Leen[a,b,c]

[a]*I-Form Advanced Manufacturing Research Centre, NUI Galway, Galway, H91 HX31, Ireland*
[b]*Mechanical Engineering, NUI Galway, Galway, H91 HX31, Ireland*
[c]*Ryan Institute for Environmental, Marine and Energy Research, NUI Galway, Galway, H91 HX31, Ireland*

** Corresponding author. Tel.: +353(0)91 495955. E-mail address: xinyu.yang@i-form.ie*

Abstract

A key challenge for successful exploitation of additive manufacturing (AM) across a broad range of industries is the development of fundamental understanding of the relationships between process control and mechanical performance of manufactured components. The present work is focused on the development of predictive methods for process-structure-property control of AM. In particular, laser beam powder bed fusion (PBF-LB) is identified as a key process for manufacture of metallic AM components. Ti-6Al-4V alloy is an important metal alloy for numerous high-performance applications, including the biomedical and aerospace industries. This paper presents initial developments on a model for microstructure prediction in PBF-LB manufacturing of Ti-6Al-4V, primarily focused on solid-state phase transformation and dislocation density evolution. The motivation is to quantify microstructure variables which control mechanical behavior, including tensile strength and ductility. A finite element (FE) based model of the process is adopted for thermal history prediction. Phase transformation kinetics for transient non-isothermal conditions are adopted and implemented within a stand-alone code, based on the FE-predicted thermal histories of sample material points. The evolution and spatial variations of phase fractions, α lath width and dislocation density are presented, to provide an assessment of the resulting microstructure-sensitivity of mechanical properties.

Keywords: Additive manufacturing; Laser beam powder bed fusion; Microstructure; Phase transformation; Dislocation density

1. Introduction

Laser beam powder bed fusion (PBF-LB) is one of the most commonly used prototyping technology for additive manufacturing (AM) of metals. In contrast with conventional processing methods, it is a layer-by-layer material deposition process leading to direct component manufacturing from a 3D drawing, including intricate geometries. However, the fast heating and cooling cycles and complex heat transfer from subsequent layer deposition during PBF-LB result in a heterogeneous microstructure, including different solidification morphology, phase fraction, dislocation density etc. throughout the build [1, 2]. In this paper, the focus is on the PBF-LB process of Ti-6Al-4V alloy which is widely used in the biomedical and aerospace industries.

Conventional Ti-6Al-4V alloy is a dual phase alloy, consisting of a majority of hexagonal close packed (HCP) α phase and some body centred cubic (BCC) β phase. The solid-state phase transformation (SSPT) between α and β is diffusion-controlled for low to intermediate cooling rates. However, the typical high cooling rate during the PBF-LB process contributes to a diffusionless transformation, leading to a martensitic transformation, which in turn will introduce a fine acicular martensite phase (α'). Murr et al. [3] have shown that such PBF-LB Ti–6Al–4V components have a high yield strength but low tensile elongation (<10%). Facchini et al. [4] attributed the high strength and low ductility of PBF-LB Ti–6Al–4V to the

2351-9789
10.1016/j.promfg.2020.04.170

generation of martensite and its strong but brittle material behavior. Yang et al. [5] found that martensite has a typical hierarchical structure and is always accompanied with a high density of dislocations and the martensitic size can be controlled by the PBF-LB processing parameter. Generally, the yield strength of martensitic material showed a negative correlation of the lath width ($\sigma_y \propto 1/w$) and increased with dislocation density ($\sigma_y \propto \sqrt{\rho}$). To overcome the strength-ductility trade-off of PBF-LB Ti–6Al–4V, Xu et al. [6, 7] developed an in-situ tailoring technology by fine-tuning the processing parameters to control the martensite fraction and thus obtain a superior mechanical performance.

Although significant experimental work has been conducted on the microstructure evolution, as addressed above, the development of predictive methods based on a fundamental understanding for process-structure-property relationship during AM is necessary for industrial production. Some modeling work has been presented for SSPT [8, 9] and α lath width prediction [10, 11] for Ti-6Al-4V in welding and directed energy deposition (DED) process, but application to PBF-LB process has not been reported. In our previous work [12], we developed an integrated process-structure model for PBF-LB Ti–6Al–4V, including thermal process simulation, solidification morphology mapping, SSPT and α lath width prediction. This framework is extended here to include prediction of dislocation density evolution within the lath interiors (LI) and along lath boundaries (LB); these are key to successful prediction of mechanical properties in PBF-LB Ti–6Al–4V. The spatial variations of phase fractions and dislocation density are also presented.

2. Modeling methodology

2.1. Thermal history prediction

A finite element (FE) based model using Abaqus® for the thermal process of PBF-LB is adopted to predict the thermal history, incorporating the effect of the moving heat flux and temperature-dependent material parameters [12]. In total, five layers are modelled in the simulation and the process parameters are shown in Table 1. The predicted thermal history is compared with measured data [13] to validate the model.

Table 1. Process parameters for PBF-LB of Ti-6Al-4V [13].

Parameter	Symbol	Unit	Value
Laser beam power	P	W	50
Laser scanning speed	V	mm/s	80
Laser spot radius	r_0	μm	35
Layer thickness	h	μm	30
Build plate temperature	T_0	°C	250

2.2. SSPT prediction

Diffusion-controlled β to α transformation during a cooling period was described by a modified JMAK equation based on the work of Kelly [8] and Charles [9]. The model was discretized for the transient non-isothermal conditions of PBF-LB process:

$$F_{\alpha,i} = \left[1 - e^{-k_i\left(t_i^{\mathrm{eq}} + \Delta t\right)^{n_i}}\right]\left(F_{\alpha,i}^{\mathrm{eq}}\right)\left(F_{\beta,i-1} + F_{\alpha,i-1}\right) \quad (1)$$

where F_α and F_β are α and β phase fraction respectively, subscript i denotes the current time step, k and n are kinetic parameters obtained from TTT curves, F_α^{eq} is the experimental equilibrium α phase fraction and t^{eq} is the equilibrium time for a transformation to start, defined as:

$$t_i^{\mathrm{eq}} = \left[-\ln\left(1 - \frac{F_{\alpha,i-1}/F_{\alpha,\mathrm{i}}^{\mathrm{eq}}}{F_{\beta,i-1} + F_{\alpha,i-1}}\right)/k_i\right]^{1/n_i} \quad (2)$$

Diffusionless β to α' transformation occurs when the temperature goes below the martensite start temperature (M_s, 575 °C) with a cooling rate larger than 410 °C/s [14]. The Koistinen–Marburger equation is used to describe the formation of α':

$$F_{\alpha',i} = \left[1 - e^{-b_{\mathrm{KM}}(M_s - T_i)}\right]\left(F_{\beta,i-1} + F_{\alpha',i-1}\right) \quad (3)$$

where $F_{\alpha'}$ is the α' phase fraction, b_{KM} is an experimental material parameter, T is the transient temperature.

During the heating cycle, α' will decompose into α and β. A similar formula to Eq. (1) is applied to the dissolution of α':

$$F_{\alpha',i} = F_{\alpha',i}^{\mathrm{eq}} - \left[e^{-k_{\alpha',i}\left(t_{\alpha',i}^{\mathrm{eq}} + \Delta t\right)^{n_{\alpha',i}}}\right]\left(F_{\alpha',i-1} + F_{\beta,i-1} - F_{\alpha',i}^{\mathrm{eq}}\right) \quad (4)$$

The α to β transformation is defined as [9]:

$$F_{\beta,i} = F_{\beta,i}^{\mathrm{eq}} r_{\beta,i}\sqrt{\Delta t + t_{\beta,i}^{\mathrm{eq}}} \quad (5)$$

where $r_{\beta,i}$ is a temperature-dependent parabolic rate, equilibrium time t_β^{eq} is defined as:

$$t_{\beta,i}^{\mathrm{eq}} = \left(\frac{F_{\beta,i-1}}{F_{\beta,i}^{\mathrm{eq}} r_{\beta,i}}\right)^2 \quad (6)$$

The implementation of the SSPT model is described in detail elsewhere [12].

2.3. α lath width prediction

The α lath width is a key microstructural parameter for prediction of mechanical properties of PBF-LB Ti–6Al–4V [7, 15]. α and α' both have a HCP structure and most retained α in as-built Ti–6Al–4V is tempered from α'. The crystallographic difference between α lath and α' lath is not considered here, and it is assumed that the lath width depends on the total α phase [11]:

$$w_i = \frac{1}{F_{\alpha,i}}\left[w_{i-1}F_{\alpha,i-1} + w_{\mathrm{eq},i}\left(F_{\alpha,i} - F_{\alpha,i-1}\right)\right] \quad (7)$$

where w_{eq} is the equilibrium α lath width, expressed as:

$$w_{\mathrm{eq},i} = k_w \exp(-T_{\mathrm{act}}/T_i) \quad (8)$$

where k_w is the Arrhenius pre-exponential factor and T_{act} is the activation temperature.

2.4. Dislocation density evolution

The primary distinction between PBF-LB Ti–6Al–4V and conventional Ti–6Al–4V is the formation of martensite in PBF-LB Ti–6Al–4V. As martensite tends to have a high dislocation density, with a value dependent on lath structure, an estimation method is developed here to evaluate the dislocation density of α'. Considering the piled-up effect of dislocation on the lath boundary (LB), the α' lath is divided into an interior part and a boundary part, to calculate dislocation density.

Dislocation density in the α' lath interior (LI) is obtained by estimating the net strain energy stored by dislocations in LI [16, 17]:

$$\rho_{\mathrm{LI}} = \frac{12E_{\alpha'}s_{\alpha'}}{(1+2\nu^2)\mu_{\alpha'}b_{\alpha'}}\frac{\varepsilon_{\mathrm{trans}}^2}{w_{\alpha'}^2} \quad (9)$$

where $E_{\alpha'}$ is the Young's modulus of α', $s_{\alpha'}$ is LB thickness, ν is Poisson's ratio, $\mu_{\alpha'}$ is shear modulus of α', $b_{\alpha'}$ is Burgers vector of α', $\varepsilon_{\mathrm{trans}}$ is transformation strain from β to α' and $w_{\alpha'}$ is lath width.

In the current approach, it is assumed that the lath is a rectangular structure with the out-plane dimension equal to the lath width [18, 19] and the aspect ratio between lath length and width ($R = l_{\alpha'}/w_{\alpha'}$) is assumed to be 26 [5]. The dislocation density on α' LB can be expressed as [19]:

$$\rho_{\mathrm{LB}} = \frac{\Lambda_{\mathrm{L}}P_{\mathrm{L}}}{2A_{\mathrm{L}}} \quad (10)$$

where Λ_{L} is the number of LB dislocations per metre of boundary, P_{L} is the lath perimeter and A_{L} is the LB section area and $s_{\alpha'}$ is used here to define the spacing between two LB dislocation, such that Λ_{L} is the reciprocal of $s_{\alpha'}$:

$$\Lambda_{\mathrm{L}} = \frac{1}{s_{\alpha'}} \quad (11)$$

$$P_{\mathrm{L}} = 4(l_{\alpha'} + w_{\alpha'} + w_{\alpha'}) \quad (12)$$

$$A_{\mathrm{L}} = 4t_{\alpha'}\left(l_{\alpha'} + w_{\alpha'} + w_{\alpha'} - \frac{3}{2}s_{\alpha'}\right) \quad (13)$$

Then the total dislocation density of α' lath can be defined as:

$$\rho_{\alpha'} = \rho_{\mathrm{LI}}F_{\mathrm{LI}} + \rho_{\mathrm{LB}}(1 - F_{\mathrm{LI}}) \quad (14)$$

where F_{LI} is the volume fraction of LI:

$$F_{\mathrm{LI}} = \frac{(l_{\alpha'} - t_{\alpha'})(w_{\alpha'} - t_{\alpha'})(w_{\alpha'} - s_{\alpha'})}{l_{\alpha'}w_{\alpha'}w_{\alpha'}} \quad (15)$$

The dislocation density of α and β are assumed to equal the value of wrought Ti–6Al–4V, ρ_{w}. Thus, the total dislocation density ρ_{total} can be expressed as:

$$\rho_{\mathrm{total}} = \rho_{\alpha'}F_{\alpha'} + \rho_{\mathrm{w}}(1 - F_{\alpha'}) \quad (16)$$

The complete set of material parameters are presented in Table 2.

Table 2. Material parameter for dislocation density evolution.

Symbol	Unit	Value	Source
$E_{\alpha'}$	GPa	108	[20]
$t_{\alpha'}$	nm	10	[21]
ν	-	0.34	[22]
$\mu_{\alpha'}$	GPa	40.4	[23]
$b_{\alpha'}$	nm	0.29	[24]
$\varepsilon_{\mathrm{trans}}$	-	0.1	[25]
ρ_{w}	m^{-2}	4×10^{13}	[3]

3. Results

Fig. 1 shows the selected sample points from the top, middle, and bottom segments of the powder bed set up in the simulation.

Fig. 2 shows the thermal history for the three selected points during printing. The critical phase transformation temperatures are included, where T_{L} is liquidus temperature; T_{S} is solidus temperature; T_{β} is β transus point and M_{s} is martensite start temperature. The SSPT is determined by the peak temperature for each thermal cycle and the different cooling rates.

In order to predict the phase fraction of the final material, the thermal history from as-built state (immediately post-print) to room temperature is presented in Fig. 3. It takes about 200 s to cool from the as-built temperature and the selected sample points have very similar cooling conditions. The time scale is significantly larger than that of the thermal history during printing.

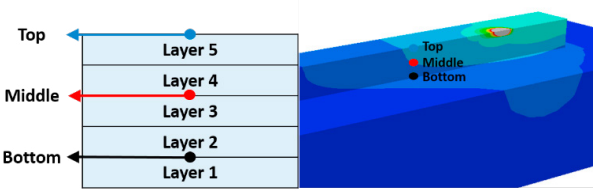

Fig. 1. The location of sample points from top, middle and bottom.

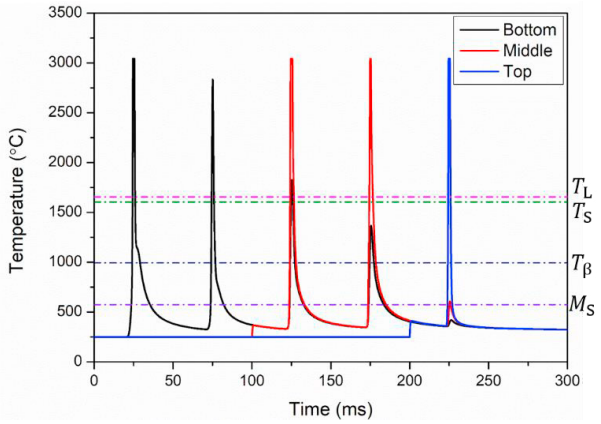

Fig. 2. Thermal history for the sample point during printing.

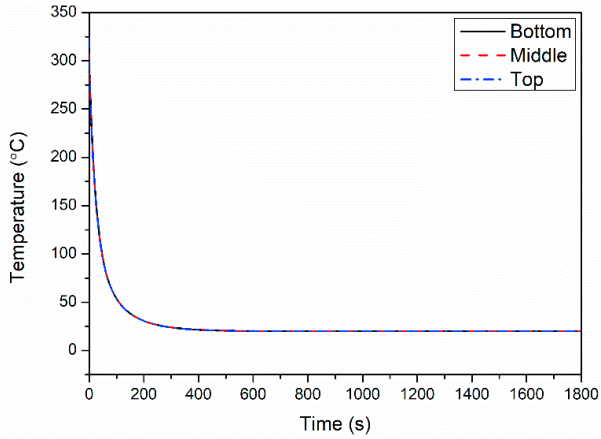

Fig. 3. Thermal history for cooling to room temperature.

Using the predicted thermal history as input data, a stand-alone code based on the developed SSPT model is developed to compute the different phase fractions of α, β and α' with the results shown in Fig. 4. And the final phase fractions for different points are presented in Table 3.

It is clear that the top point is almost fully martensite with the largest α' fraction of 92.8%, 7.1% of β, and the α phase fraction is negligible. In the middle, α is about twice the retained α' and the β is the lowest at approx. 3.4%. The bottom point experienced the most complex thermal cycle, with a similar β fraction to the top point, with 4% α' dissolved to α.

Fig. 5 shows the predicted lath width. In general, the middle point has the largest lath width while the top and bottom point share the same final value. The predicted lath width is consistent with the experimentally-measured data with approximate 87% in the range from 0.5 μm to 2 μm (Xiao et al. [15], although for different PBF-LB processing conditions: (a) laser beam power 400 W, (b) laser scanning speed 1500 mm/s, (c) Laser spot radius 50 μm, (d) layer thickness 50 μm.)

Based on the predicted phase fraction and lath width, the dislocation density is evaluated using the method described in Section 2.4 and the results are shown in Fig. 6. All the samples have higher dislocation density than wrought Ti–6Al–4V. The difference between the top and bottom points are very small while the dislocation density of middle point is about 60% lower. The predicted dislocation density is comparable to the measured value of about 2.4×10^{14} m^{-2} from Cottam et al. [26] in PBF-LB Ti–6Al–4V, which is of the same order of magnitude.

Table 3. Final phase fractions for selected points.

	Phase fraction (%)		
Location	α	α'	β
Top	0	92.8	7.1
Middle	60.2	36.4	3.4
Bottom	4	89.1	6.9

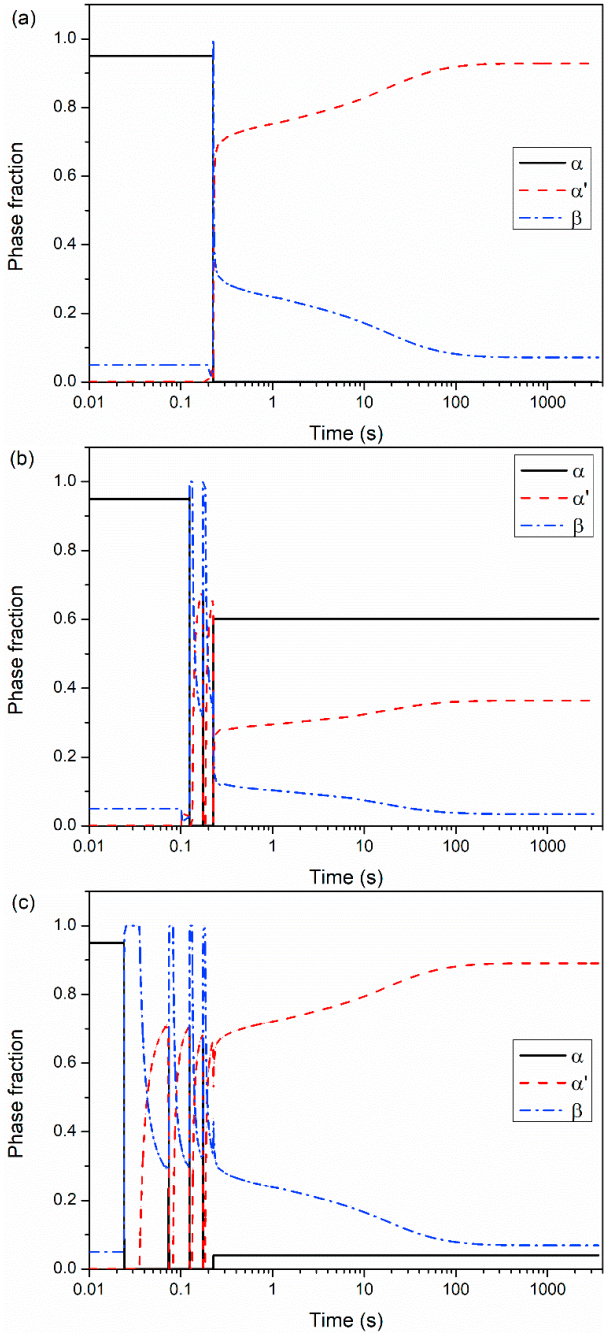

Fig. 4. Predicted phase fraction of α, β and α' for the sample points (a) top; (b) middle; (c) bottom.

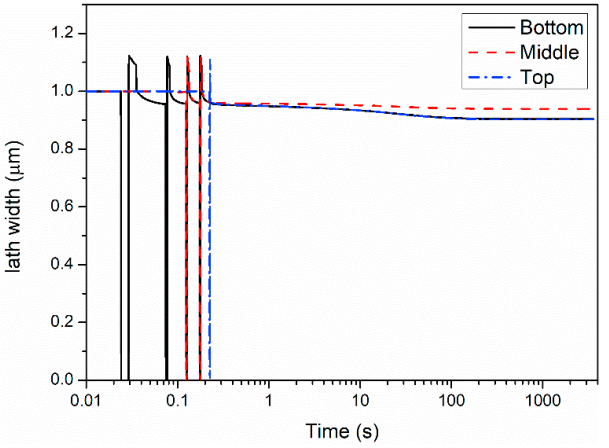

Fig. 5. Predicted lath width for the sample points.

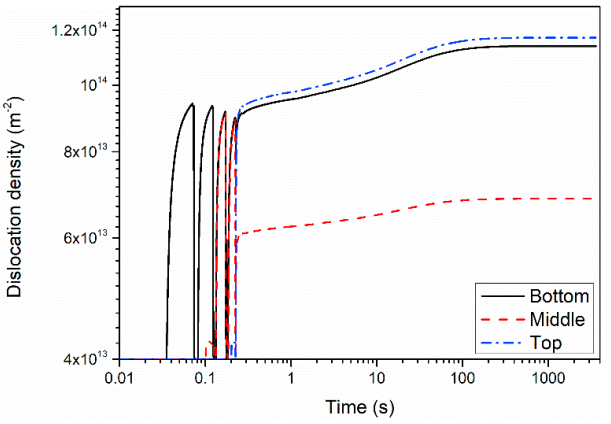

Fig. 6. Predicted dislocation density for the sample points.

4. Discussion

The prediction methodology for microstructure evolution presented in this paper provides an effective and efficient method to quantify microstructure variables which control mechanical behaviour. The predicted phase fraction shows that, in general, α' dissolves into α and β in the sample. However, on the top surface a large amount of α' was retained, due to the lack of successive deposition. This shows good agreement with the microstructural examination by Xu et al. [7] using backscattered electron (BSE). The undesired martensite can be dissolved into α and β using the heat accumulated during the thermal cycle. Moreover, the α and β transformed from α' has an ultrafine lamellar structure, which simultaneously enhances strength and ductility [7]. The developed model here can be used to predict optimal processing parameters for PBF-LB, to obtain such an ultrafine lamellar α+β structure.

In view of the fact that strength is inversely proportional to lath width and positively associated with dislocation density, the PBF-LB Ti-6Al-4V shows the potential for significant anisotropy of mechanical behavior.

5. Conclusion

A microstructural model has been developed to predict the evolution and spatial variations of phase fractions, α lath width and dislocation density in PBF-LB Ti-6Al-4V. The key conclusions that can be drawn are as follows:

- A method has been presented for prediction of microstructure-sensitivity of mechanical properties for PBF-LB of Ti-6Al-4V;
- The top segment of PBF-LB Ti-6Al-4V is predicted to have the largest martensite fraction and hence highest dislocation density;
- The model prediction for the spatial variations of phase fractions is consistent with experimental observations from the PBF-LB process. α' can dissolve in-situ to α and β using the heat accumulated during the thermal cycle;
- The quantified microstructure variables indicate the potential for significant anisotropy of microstructure and mechanical behavior for PBF-LB Ti-6Al-4V in the as-built condition.

Acknowledgements

This publication has emanated from research supported in part by a research grant from Science Foundation Ireland (SFI) under grant number 16/RC/3872 and is co-funded under the European Regional Development Fund.

References

[1] Gockel J, Sheridan L, Narra SP, Klingbeil NW, Beuth J. Trends in Solidification Grain Size and Morphology for Additive Manufacturing of Ti-6Al-4V. JOM 2017;69:2706-10.
[2] Zhao C, Fezzaa K, Cunningham RW, Wen H, De Carlo F, Chen L, et al. Real-time monitoring of laser powder bed fusion process using high-speed X-ray imaging and diffraction. Sci Rep 2017;7:3602.
[3] Murr LE, Quinones SA, Gaytan SM, Lopez MI, Rodela A, Martinez EY, et al. Microstructure and mechanical behavior of Ti–6Al–4V produced by rapid-layer manufacturing, for biomedical applications. J Mech Behav Biomed 2009;2:20-32.
[4] Facchini L, Magalini E, Robotti P, Molinari A, Höges S, Wissenbach K. Ductility of a Ti-6Al-4V alloy produced by selective laser melting of prealloyed powders. Rapid Prototyp J 2010;16:450-9.
[5] Yang JJ, Yu HC, Yin J, Gao M, Wang ZM, Zeng XY. Formation and control of martensite in Ti-6Al-4V alloy produced by selective laser melting. Mater Des 2016;108:308-18.
[6] Xu W, Lui EW, Pateras A, Qian M, Brandt M. In situ tailoring microstructure in additively manufactured Ti-6Al-4V for superior mechanical performance. Acta Mater 2017;125:390-400.
[7] Xu W, Brandt M, Sun S, Elambasseril J, Liu Q, Latham K, et al. Additive manufacturing of strong and ductile Ti-6Al-4V by selective laser melting via in situ martensite decomposition. Acta Mater 2015;85:74-84.
[8] Kelly SM. Thermal and microstructure modeling of metal deposition processes with application to Ti-6Al-4V. [Ph.D. Thesis]. USA: Virginia Tech; 2004.
[9] Charles C, Pederson R, Lindgren L-E. A model for Ti–6Al–4V microstructure evolution for arbitrary temperature changes. Modell Simul Mater Sci Eng 2012;20:055006.
[10] Charles C, Jarvstrat N. Modelling Ti-6Al-4V Microstructure by Evolution Laws Implemented as Finite Element Subroutines: Application to TIG Metal Deposition. In: al. SDe, editor. Proc The 8th International Conference on Trends in Welding Research (TWR) Pine Mountain, Georgia (USA)2009. p. 477-85.
[11] Irwin J, Reutzel EW, Michaleris P, Keist J, Nassar AR. Predicting Microstructure From Thermal History During Additive Manufacturing for Ti-6Al-4V. J Manuf Sci E-T Asme 2016;138.
[12] Yang X, Barrett RA, Tong M, Harrison NM, Leen SB. Towards a process-structure model for Ti-6Al-4V during additive manufacturing (in preparation). 2020.
[13] Karayagiz K, Elwany A, Tapia G, Franco B, Johnson L, Ma J, et al. Numerical and experimental analysis of heat distribution in the laser powder bed fusion of Ti-6Al-4V. IISE Transactions 2019;51:136-52.
[14] Ahmed T, Rack HJ. Phase transformations during cooling in alpha+beta titanium alloys. Mater Sci Eng A 1998;243:206-11.
[15] Xiao L, Song W, Hu M, Li P. Compressive properties and micro-structural characteristics of Ti–6Al–4V fabricated by electron beam melting and selective laser melting. Mater Sci Eng A 2019:138204.
[16] Frost HJ, Ashby MF. Deformation mechanism maps: the plasticity and creep of metals and ceramics: Pergamon press; 1982.
[17] Galindo-Nava EI, Rivera-Diaz-del-Castillo PEJ. A model for the microstructure behaviour and strength evolution in lath martensite. Acta Mater 2015;98:81-93.
[18] Morsdorf L, Tasan CC, Ponge D, Raabe D. 3D structural and atomic-scale analysis of lath martensite: Effect of the transformation sequence. Acta Mater 2015;95:366-77.
[19] Barrett RA, O'Donoghue PE, Leen SB. A physically-based constitutive model for high temperature microstructural degradation under cyclic deformation. Int J Fatigue 2017;100:388-406.
[20] Imam MA, Gilmore CM. Fatigue and microstructural properties of quenched Ti- 6Al- 4V. Metall Mater Trans A 1983;14:233-40.
[21] Vilaro T, Colin C, Bartout JD. As-Fabricated and Heat-Treated Microstructures of the Ti-6Al-4V Alloy Processed by Selective Laser Melting. Metall Mater Trans A 2011;42a:3190-9.
[22] Denlinger ER. Thermo-mechanical model development and experimental validation for metallic parts in additive manufacturing. [Ph.D. Thesis]. USA: The Pennsylvania State University; 2015.
[23] Fatemi A, Molaei R, Sharifimehr S, Shamsaei N, Phan N. Torsional fatigue behavior of wrought and additive manufactured Ti-6A1-4V by powder bed fusion including surface finish effect. Int J Fatigue 2017;99:187-201.
[24] Tan X, Kok Y, Toh WQ, Tan YJ, Descoins M, Mangelinck D, et al. Revealing martensitic transformation and α/β interface evolution in electron beam melting three-dimensional-printed Ti-6Al-4V. Sci Rep 2016;6:26039.
[25] Galindo-Nava EI. On the prediction of martensite formation in metals. Scripta Mater 2017;138:6-11.
[26] Cottam R, Palanisamy S, Avdeev M, Jarvis T, Henry C, Cuiuri D, et al. Diffraction Line Profile Analysis of 3D Wedge Samples of Ti-6Al-4V Fabricated Using Four Different Additive Manufacturing Processes. Metals 2019;9.